ChemPubSoc Europe

DOI: 10.1002/chem.201402632

CHEMISTRY A European Journal Full Paper

Femtochemistry

# Impact of Metal Ions in Porphyrin-Based Applied Materials for Visible-Light Photocatalysis: Key Information from Ultrafast Electronic Spectroscopy

Prasenjit Kar,[a] Samim Sardar,[a] Erkki Alarousu,[b] Jingya Sun,[b] Zaki S. Seddigi,[c] Saleh A. Ahmed,[d] Ekram Y. Danish,[e] Omar F. Mohammed,*[b] and Samir Kumar Pal*[a]

**Abstract:** Protoporphyrin IX-zinc oxide (PP-ZnO) nanohybrids have been synthesized for applications in photocatalytic devices. High-resolution transmission electron microscopy (HRTEM), X-ray diffraction (XRD), and steady-state infrared, absorption, and emission spectroscopies have been used to analyze the structural details and optical properties of these nanohybrids. Time-resolved fluorescence and transient absorption techniques have been applied to study the ultrafast dynamic events that are key to photocatalytic activities. The photocatalytic efficiency under visible-light irradiation in the presence of naturally abundant iron(III) and copper(II) ions has been found to be significantly retarded in the former case, but enhanced in the latter case. More importantly, femtosecond (fs) transient absorption data have clearly demonstrated that the residence of photoexcited electrons from the sensitizer PP in the centrally located iron moiety hinders ground-state bleach recovery of the sensitizer, affecting the overall photocatalytic rate of the nanohybrid. The presence of copper(II) ions, on the other hand, offers additional stability against photobleaching and eventually enhances the efficiency of photocatalysis. In addition, we have also explored the role of UV light in the efficiency of photocatalysis and have rationalized our observations from femtosecond- to picosecond-resolved studies.

## Introduction

Sensitization of wide-band-gap semiconductors by organic dyes for all kinds of solar devices is an essential requirement.[1] The design of low-cost and environmentally friendly "green" dye-sensitized nanoparticle-based solar-light-harvesting devices relies on the nature of the organic dyes used as light-absorbing materials. A considerable research effort in this direction stems from the desire to tackle a number of problems, including cost and environmental compatibility.[2] The synthesis and purification of the best-performing ruthenium-based dyes for solar-light-harvesting devices is expensive. For example, terpyridine black dye sells for around $3500 per gram.[3] The second problem is the phototoxicity of ruthenium-based dyes, raising potential environmental hazards.[4] A detailed study of the mechanism of phototoxicity of $[Ru(phen)_3]^{2+}$ dyes has shown that upon illumination, extracellular and membrane-bound $Ru^{II}$ complexes generate singlet oxygen molecules. A high local concentration of singlet oxygen molecules causes a sequence of undesirable events that eventually leads to plasma membrane damage, which is manifested in a loss of membrane integrity and entry of the dye into living cells.[5] In optimizing the balance between cost and biocompatibility, porphyrin-based solar devices are attracting interest in the contemporary literature.[6] Recently, Chen et al.[7] demonstrated a significant enhancement in visible-light photocatalysis upon attachment of porphyrin (*meso*-tetra(*p*-hydroxyphenyl)porphyrin; *p*-THPP) nanoparticles (NPs) to macroscopic graphene (reduced graphene oxide; rGO) films. The use of porphyrins from natural sources (hematoporphyrin, protoporphyrin) in solar devices has been reported to meet the requirements relating to cost and toxicity.[8] Our previous studies on hematoporphyrin-sensitized ZnO nanorods indicated dual applications in efficient visible-light photocatalysis (VLP) and dye-sensitized solar cells (DSSC).[9] ZnO nanoparticles are considered to be nontoxic and

[a] *P. Kar,[+] S. Sardar,[+] Prof. S. K. Pal*
*Department of Chemical, Biological and Macromolecular Sciences*
*S. N. Bose National Centre for Basic Sciences*
*Block JD, Sector III, SaltLake, Kolkata 700 098 (India)*
*Fax: (+033) 2335-3477*
*E-mail: skpal@bose.res.in*

[b] *Dr. E. Alarousu, Dr. J. Sun, Dr. O. F. Mohammed*
*Solar and Photovoltaics Engineering Research Center*
*Division of Physical Sciences and Engineering*
*King Abdullah University of Science and Technology*
*Thuwal 23955-6900 (Saudi Arabia)*
*E-mail: Omar.Abdelsaboor@kaust.edu.sa*

[c] *Prof. Z. S. Seddigi*
*Department of Environmental Health*
*Faculty of Public Health and Health informatics*
*Umm Al-Qura University, 21955 Makkah (Saudi Arabia)*

[d] *Prof. S. A. Ahmed*
*Chemistry Department, Faculty of Applied Sciences*
*Umm Al-Qura University, 21955 Makkah (Saudi Arabia)*

[e] *Dr. E. Y. Danish*
*Chemistry Department, College of Sciences*
*King Abdulaziz University, Jeddah (Saudi Arabia)*

[+] *These authors contributed equally to this work.*

biocompatible, and have been used in many applications in our daily lives, including as drug carriers and in cosmetics.[10] The role of metal ions in the central cavity of the porphyrin in the proximity of the host semiconductor for efficient decontamination of drinking water has been a subject of several recent reports.[11] Tuning the photo-response,[12] the efficiency of photo-injected electrons,[13] and the stability of dyes upon metalation[14] have been addressed in a series of reports.[15] In our recent studies, we explored the critical role of the central metal ions ($Fe^{3+}/Fe^{2+}$) incorporated into hematoporphyrin-$TiO_2$ nanohybrids and their implications in photocatalysis.[16]

From the practical application point of view, the use of porphyrin-based photocatalytic devices for water decontamination is very important, given the fact that water from natural resources contains metal ions (especially $Fe^{3+}$ and $Cu^{2+}$). In the present study, we have synthesized and characterized a PP-ZnO nanohybrid for a flow-type photocatalytic solar device for a prototype water decontamination plant using visible light. We have explored the role of metal ions, specifically iron(III) and copper(II), in the test water, and have deployed a model contaminant, methylene blue (MB), a hazardous waste product from the textile industry,[17] in the photocatalytic device under visible light. Femtosecond time-resolved transient absorption studies have clearly unraveled the key time component associated with ground-state recovery of the sensitized PP upon metalation for the change in overall photocatalytic efficiency. In addition, picosecond-resolved fluorescence studies of the nanohybrids in the absence and presence of metal ions have clearly shown that excited-state electron-transfer dynamics is responsible for the photocatalytic action. Moreover, the role of UV light excitation of the nanohybrid, in which the host semiconductor is expected to be excited, is also discussed. Our studies are expected to be of relevance to the large-scale use of porphyrin-based nanomaterials for the decontamination of drinking water by solar light catalysis.

## Results and Discussion

### Structural characterization of the nanohybrids

A typical high-resolution transmission electron microscope (HR-TEM) image of ZnO NPs is shown in Figure 1a. From the TEM study, an average size of the ZnO NPs of 25 nm was estimated. TEM study of a single NP revealed crystal fringes with an interplanar distance of 0.26 nm (inset in Figure 1a), corresponding to the spacing between two (002) planes of ZnO.[18] XRD study (Figure 1b) on the bare ZnO NPs (2θ range from 20° to 70°) and upon sensitization with PP, in the absence and presence of the metal ions ($Fe^{III}$, $Cu^{II}$), showed the characteristic planes of ZnO (100), (002), (101), (102), (110), and (103). Intactness of the crystal planes of ZnO upon sensitization of the PP dye and metal ions was also clear from this study. Wurtzite ZnO exhibits well-defined crystallographic faces, that is, polar (002) and nonpolar (100), (101) surfaces. McLaren et al.[19] showed the terminal polar faces to be more active surfaces for photocatalysis than the nonpolar surfaces perpendicular to them.

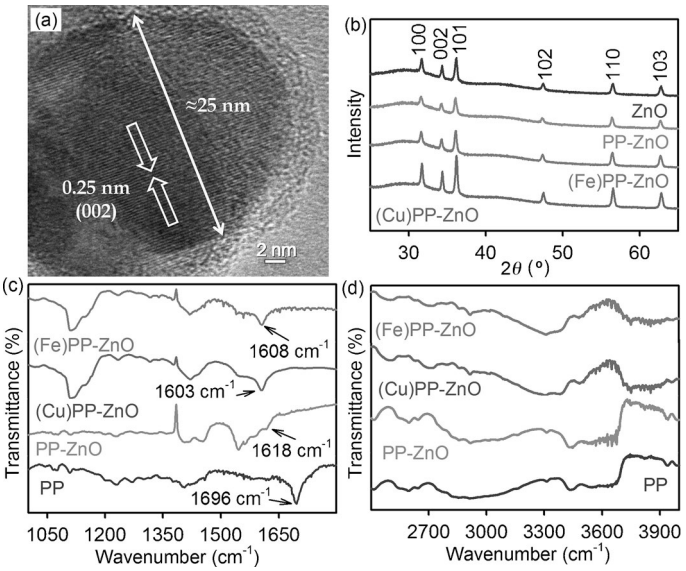


**Figure 1.** (a) HRTEM images of ZnO NPs. (b) X-ray diffraction patterns of ZnO, PP-ZnO, (Fe)PP-ZnO, (Cu)PP-ZnO. (c) FTIR spectra of PP, PP-ZnO, (Cu)PP-ZnO, (Fe)PP-ZnO. The spectra of PP-ZnO, (Fe)PP-ZnO, and (Cu)PP-ZnO were taken on a ZnO background. (d) FTIR spectra of PP, PP-ZnO, (Cu)PP-ZnO, and (Fe)PP-ZnO.

### FTIR study

Fourier-transform infrared (FTIR) spectroscopy was used to confirm the binding mode of PP on the ZnO surface. For free PP, stretching frequencies of the carboxylic group are located at 1696 and 1402 $cm^{-1}$ for the antisymmetric and symmetric stretching vibrations, respectively, as shown in Figure 1c. In PP-ZnO, the stretching frequencies of the carboxylic groups are located at 1618 and 1405 $cm^{-1}$ for the antisymmetric and symmetric stretching vibrations, respectively, providing clear evidence for deprotonation of the carboxylic group upon addition of ZnO NPs. The difference between the carboxylate stretching frequencies, $\Delta = \nu_{as} - \nu_{sym}$, is useful in identifying the binding mode of the carboxylate ligand.[20] The observed $\Delta$ value for the PP-ZnO nanohybrid was 213 $cm^{-1}$, smaller than that of free PP (294 $cm^{-1}$). This suggests that the binding mode of PP on ZnO is predominantly bidentate. However, nanohybrids incorporating $Fe^{III}$ and $Cu^{II}$ also show bidentate covalent binding of PP to ZnO NPs through the carboxylic groups. The N–H stretching frequency has been used to investigate the attachment of the metal ions to the PP associated with the ZnO host. In free PP, the N–H stretching frequency is at 3441 $cm^{-1}$ (Figure 1d). In the case of the PP-ZnO nanohybrid, the N–H stretching frequency of the PP cavity remains unperturbed as PP anchors onto the ZnO surface through its carboxylic group. In the presence of iron or copper, the N–H bond is perturbed, indicating that iron(III) and copper(II) bind to the PP through the pyrrole nitrogen atoms of the porphyrin.[16] The binding between PP and ZnO was also confirmed by Raman spectroscopy. Raman spectra were collected from PP, ZnO NPs, and PP-ZnO nanohybrids in the wavenumber region 300–600 $cm^{-1}$. PP molecules do not show an obvious peak in the experimental range. However, four vibration peaks at 328,

378, 438, and 577 $cm^{-1}$ are observed in the Raman spectrum of ZnO NPs, indicating the presence of a wurtzite structure. The strong peak at 438 $cm^{-1}$ can be assigned to the nonpolar optical phonon, $E_2$, mode of the ZnO NPs at high frequency, which is associated with oxygen deficiency.[21] Noticeably, the characteristic band of the $E_2$ mode of ZnO shifts towards lower wavenumber and its linewidth is larger upon its attachment to PP. This indicates passivation of the ZnO surface states upon PP assembly.

### Steady-state optical study of the nanohybrid

With extensively delocalized π electrons, PP exhibits a Soret band ($S_0 \rightarrow S_2$) and Q bands ($S_0 \rightarrow S_1$) due to its π–π* electronic transition. UV/Vis absorption spectra of PP in DMSO/water clearly indicate the formation of H-type and J-type aggregates due to the presence of peaks at 352 and 465 nm, respectively (Figure 2a).[22] The Soret band peak of PP appears at 405 nm, whereas the Q-band peaks are observed in the range between 500 and 650 nm. The disappearance of the aggregate peak at 463 nm and the red-shift in the Soret band (405 to 421 nm in Figure 2a) are indicative of direct interaction of PP with ZnO nanoparticles.[8c,23] As shown in Figure 2b, PP in DMSO/water exhibits strong emissions at 630 and 700 nm upon excitation at the Soret band by a laser source at 409 nm. However, after metalation with $Fe^{III}$ and $Cu^{II}$, steady-state emission of PP is significantly decreased, indicating non-radiative processes that can be attributed to fast intersystem crossing to the excited triplet state.[24] In addition, charge-transfer processes have also been demonstrated to be responsible for the quenching.[25]

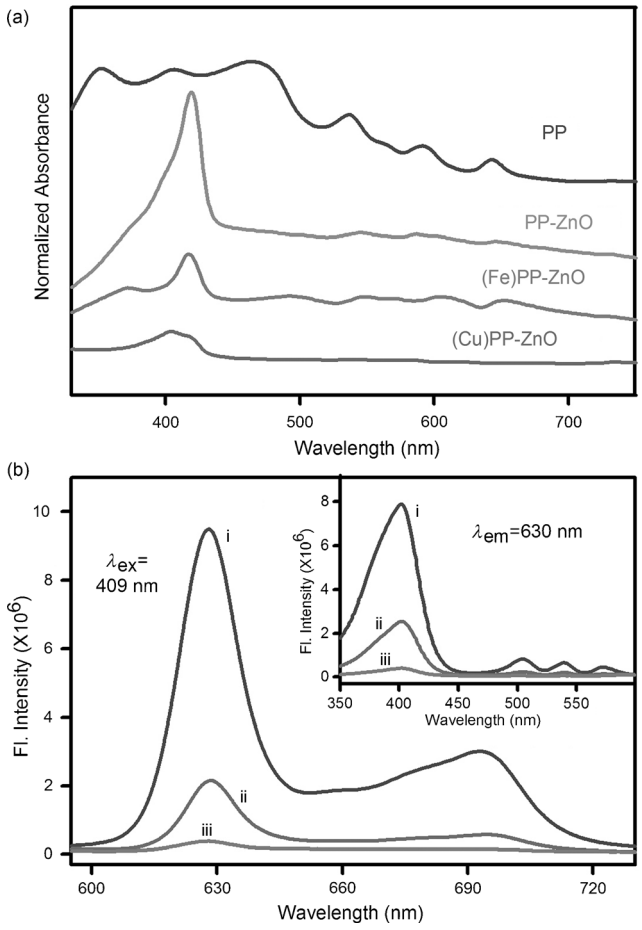


**Figure 2.** (a) UV/Vis absorption spectra of PP, PP-ZnO, (Fe)PP-ZnO, and (Cu)PP-ZnO in DMSO/water (1:1, v/v). (b) Room temperature PL spectra of PP (i), PP-Cu (ii), and PP-Fe (iii) in DMSO/water (1:1, v/v). The inset shows excitation spectra monitored at 630 nm.

### Visible-light photocatalysis by the nanohybrid and the effect of dissolved metal ions

Figure 3a shows a prototype photodevice for investigation of the photocatalytic efficiency of the nanohybrid under visible-light irradiation. Full details of the device may be found in our earlier publication.[26] The test water under investigation contained methylene blue (MB), a model water contaminant, in the absence and presence of iron and copper cations (44.5 mg $L^{-1}$ copper and 39.2 mg $L^{-1}$ iron). From the data shown in Figure 3b, the presence of iron ions in the water significantly decreased the photocatalytic efficiency, whereas copper enhanced the degradation of MB within our experimental time window of two hours. Our observations are consistent with previous literature reports.[14,16] Oliveros et al.[8c] investigated the photodegradation of atrazine in an aqueous solution under visible-light irradiation in the presence of tetra(4-carboxyphenyl)porphyrin (TcPP) in the absence/presence of different central metal ions ($Fe^{III}$, $Cu^{II}$, $Zn^{II}$) adsorbed on a $TiO_2$ surface, and the maximum photocatalytic activity was obtained using $Cu^{II}$ porphyrin as the photosensitizer after the addition of hydrogen peroxide. The concentrations of metal ions used here (44.5 mg $L^{-1}$ copper and 39.2 mg $L^{-1}$ iron) are of the order of those recommended by the World Health Organization (WHO) in drinking water (30 mg $L^{-1}$ copper and 10 mg $L^{-1}$ iron) available from natural resources. In the photocatalytic reaction, MB reacts with the conduction-band electron of ZnO to form a well-known colorless product, leuco methylene blue (LMB),[27] as shown in Equation (1):

$$2\,MB + 2\,e^- + H^+ = MB + LMB \quad (1)$$

The energy-dispersive X-ray analysis (EDAX) spectra of PP-ZnO before and after two hours of photocatalysis in the presence of copper(II) and iron(III) ions are shown in Figure 3c–e. These spectra clearly indicate the presence of metal ions on the catalyst surface after the photocatalysis. The complexation rate of copper with PP is higher than that of iron, which leads to the presence of more copper (4.95%) on PP-ZnO than iron (1.52%).[28] To confirm the complex formation, FTIR studies were conducted as shown in Figure 3f. For PP-ZnO, the N–H stretching frequency is at 3441 $cm^{-1}$. In the presence of iron and copper, the N–H band is broadened and shifted to 3385 $cm^{-1}$, suggesting that iron(III) and copper(II) bind to the PP through the pyrrole nitrogen atoms of the porphyrin. Thus, the metal ions present in the contaminant solution are complexed with PP. After two hours of photocatalysis, around 5–10% PP had leached out from the ZnO surface.

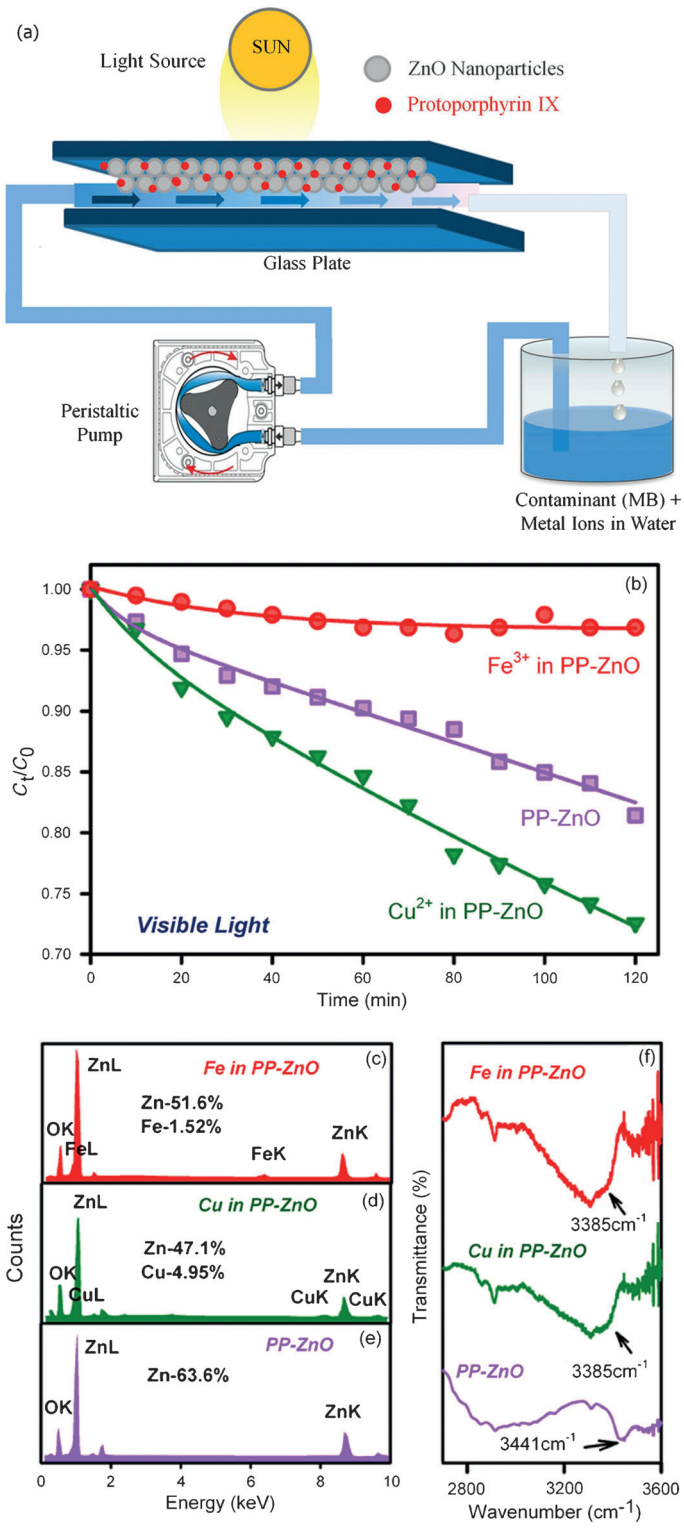


**Figure 3.** (a) Schematic representation of the flow device developed for photocatalysis. (b) Photocatalytic degradation of MB in the flow device using PP-ZnO as the photocatalyst in the presence of $Cu^{2+}$ (dark green) or $Fe^{3+}$ (red) as contaminants in MB solution and without any metal ions (pink). EDAX spectra of PP-ZnO (pink, e) in the presence of $Cu^{2+}$ (dark green, d), and $Fe^{3+}$ (red, c). (f) FTIR spectra of PP-ZnO (pink) before photocatalysis and after photocatalysis in the presence of $Cu^{2+}$ (dark-green) and $Fe^{3+}$ (red).

To the best of our knowledge, such studies revealing the role of metal ions in test water in the photocatalytic activity of porphyrin-based nanohybrids and a detailed understanding of the molecular mechanism of photocatalysis have been rare in the literature. Hence, we identified a need for exploration of ultrafast dynamic studies on the nanohybrid.

### Femtosecond broadband transient absorption study

Femtosecond-resolved transient absorption spectra (excitation wavelength 350 nm) of the PP-ZnO nanohybrid in the presence and absence of iron and copper ions in the wavelength range 360–440 nm are shown in Figure 4a–c. It should be noted that the peaks at 370 nm and around 415 nm correspond to the band gap of the ZnO host (3.37 eV) and the

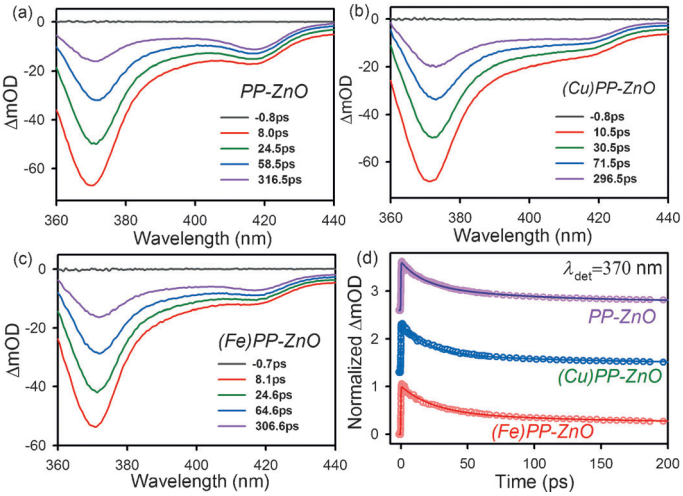


**Figure 4.** Transient absorption spectra of (a) PP-ZnO, (b) (Cu)PP-ZnO, and (c) (Fe)PP-ZnO at different time delays after excitation at 350 nm. (d) Time-resolved absorption changes of PP-ZnO (pink), (Cu)PP-ZnO (blue), and (Fe)PP-ZnO (red) at a probe wavelength of 370 nm. All spectra were recorded in DMSO/water (1:1, v/v).

Soret band of the PP guest, respectively. Decay profiles at a detection wavelength of 370 nm, revealing ground-state recovery of the excited ZnO in the nanohybrid in the presence and absence of the metal ions, are shown in Figure 4d. The possibility of interference by the absorption of PP at the detection wavelength (370 nm) was ruled out through a set of control experiments with pure PP, which revealed different time scales (of the order of ns) for ground-state bleach recovery. Numerical fitting of the transient absorption data of PP-ZnO gave decay time constants of 16.91 ps (48.63%), 88.64 ps (34.14%), and 7.44 ns (17.27%) for the ground-state recovery of the ZnO host in the nanohybrid. The nanohybrid in the presence of copper ions showed similar recovery time constants (16.20 ps (51.10%), 90.00 ps (30.98%), and 7.85 ns (17.92%)), but a significant retardation was observed in the presence of iron ions (25.00 ps (58.29%), 204.23 ps (22.99%), and 11.01 ns (18.72%)).

These time constants imply that iron ions can efficiently separate the electron–hole pairs of the excited ZnO NPs, leading to slow recovery of the ground state of the ZnO NPs in the nanohybrid. Transient absorption spectra of the Q bands of PP in the nanohybrids in the wavelength range 465–660 nm are

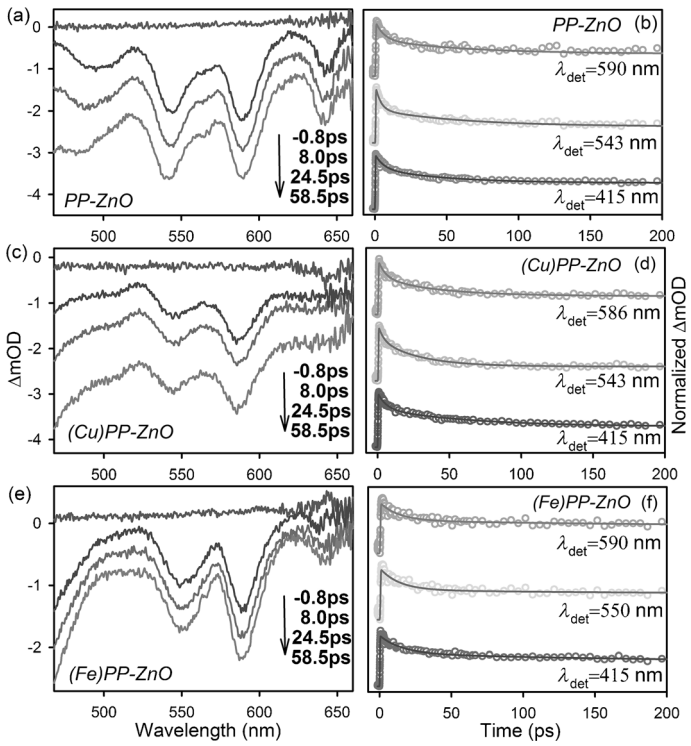


**Figure 5.** Transient absorption spectra of (a) PP-ZnO, (c) (Cu)PP-ZnO, and (e) (Fe)PP-ZnO at different time delays after excitation at 350 nm. Time-resolved absorption changes of (b) PP-ZnO, (d) (Cu)PP-ZnO, and (f) (Fe)PP-ZnO at different probe wavelengths. All spectra were recorded in DMSO/water (1:1, v/v).

shown in Figure 5 a, c, and e. From these spectra, it is evident that the four Q bands seen for the free base PP essentially merged into two in the presence of iron(III) or copper(II) ions due to the higher molecular symmetry ($D_{4h}$).[29] The decay profiles in the Soret and Q bands, revealing the ground-state recovery of the excited PP in the nanohybrid in the presence and absence of metal ions, are shown in Figure 5 b, d, f. The decay time constants are presented in Table 1. Table 1 and Figure 5 clearly indicate that the presence of iron(III) ions delays the recovery of the excited PP, whereas the presence of copper ions does not significantly affect the time constants of PP compared to those in the nanohybrid. From the above observations on the ground-state recovery dynamics, upon UV excitation of ZnO in the nanohybrid in the presence of iron ions, charge transfer is expected to be facilitated (longer exciton lifetime), leading to improved photocatalysis.[30]

### Picosecond-resolved fluorescence studies

The fluorescence decays of PP and the PP-ZnO nanohybrid, monitored at 630 nm following excitation at 409 nm, in the absence and presence of iron(III) and copper(II) ions, are shown in Figure 6 a and b (shorter time window). The fluorescence transients of PP and (Cu)PP could be fitted with single exponential decays with lifetimes of 16.03 and 17.29 ns, respectively (Table 2). The increase in the excited-state lifetime of PP in the presence of copper ions may be indicative of the stability of the PP molecule, as reported previously.[14] The time-resolved data for (Cu)PP exclude the possibility of charge-transfer transitions from PP to $Cu^{II}$ ions, and thus the steady-state quenching of the PP emission in the presence of $Cu^{II}$ can be attributed to fast intersystem crossing, which is outside of our experimental time window.[24] However, the fluorescence decay profile of PP in the presence of iron(III) shows shorter time constants of 0.048 ns (50 %) and 2.34 ns (5.95 %) along with 16.61 ns (44.05 %), with an average excited-state lifetime of 7.48 ns. The shorter excited-state lifetime of PP in the presence of iron ions could be correlated to the electron-transfer process from the former to the latter.[16] The apparent nonradiative rate constant ($k_{nr}$)[31] was determined by comparing the lifetimes of PP in the absence ($\tau_0$) and the presence ($\tau$) of an acceptor, by using the following equation:

$$k_{nr} = 1/\langle\tau\rangle - 1/\langle\tau_0\rangle \quad (2)$$

As shown in Figure 6, in the PP-ZnO nanohybrid, the fluorescence decay profile is composed of a faster component of 2.06 ns (56.25 %) and a slower component of 16.77 ns (43.75 %), indicating an electron-transfer process from PP molecules to the ZnO NPs. Although the slower component is consistent with the excited-state lifetime of PP without ZnO, the faster one may be rationalized as the electron migration time from PP to the ZnO host.[32] In the presence of copper(II) ions, the excited-state dynamics of the nanohybrid remains essentially unaltered. However,

**Table 1.** Fits of the transient absorption data at different probe wavelengths.

| Sample | Monitored wavelength [nm] | $\tau_1$ [ps] | $\tau_2$ [ps] | $\tau_3$ [ns] |
|---|---|---|---|---|
| PP-ZnO | 370 | 16.91 (48.63 %) | 88.64 (34.14 %) | 7.44 (17.27 %) |
| | 415 | 6.00 (24.44 %) | 45.81 (26.54 %) | 1.60 (49.02 %) |
| | 543 | 3.73 (40.05 %) | 60.00 (29.92 %) | 1.60 (30.03 %) |
| | 590 | 5.84 (31.68 %) | 60.00 (26.11 %) | 1.60 (42.21 %) |
| (Cu)PP-ZnO | 370 | 16.20 (51.10 %) | 90.00 (30.98 %) | 7.85 (17.92 %) |
| | 415 | 5.69 (27.87 %) | 61.45 (33.27 %) | 1.60 (38.86 %) |
| | 543 | 3.59 (23.68 %) | 27.52 (49.70 %) | 1.60 (26.62 %) |
| | 586 | 5.10 (31.20 %) | 40.93 (33.64 %) | 1.60 (35.16 %) |
| (Fe)PP-ZnO | 370 | 25.00 (58.29 %) | 204.23 (22.99 %) | 11.01 (18.72 %) |
| | 415 | 15.00 (34.16 %) | 201.73 (17.90 %) | 1.60 (47.94 %) |
| | 550 | 13.41 (41.38 %) | 200.00 (7.56 %) | 1.60 (51.06 %) |
| | 590 | 13.06 (34.31 %) | 220.00 (11.82 %) | 1.60 (53.87 %) |

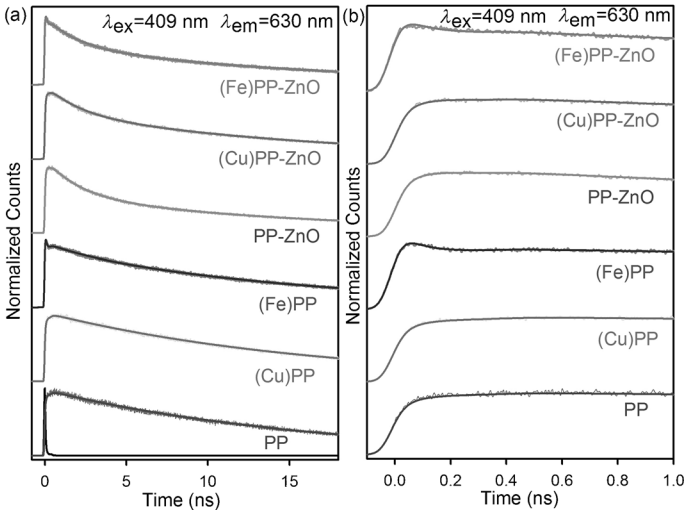


**Figure 6.** Fluorescence decay profiles of PP, (Cu)PP, (Fe)PP, PP-ZnO, (Cu)PP-ZnO, and (Fe)PP-ZnO with (a) a longer time window and (b) a shorter time window. All spectra were recorded in DMSO/water (1:1, v/v).

**Table 2.** Picosecond-resolved fluorescence transients of PP, (Fe)PP, (Cu)PP, PP-ZnO, (Fe)PP-ZnO, and (Cu)PP-ZnO composites.[a]

| Sample | $\tau_1$ [ns] | $\tau_2$ [ns] | $\tau_3$ [ns] | $\tau_{av}$ [ns] | $k_{nr}\times10^7$ [$s^{-1}$] |
|---|---|---|---|---|---|
| PP | 16.03 ±0.01 (100%) | | | 16.03 ±0.01 | |
| (Fe)PP | 16.61 ±0.05 (44.05%) | 2.34 ±0.10 (5.95%) | 0.048 ±0.001 (50%) | 7.48 ±0.03 | 7.12±0.05 |
| (Cu)PP | 17.29 ±0.01 (100%) | | | 17.29 ±0.01 | |
| PP-ZnO | 16.77 ±0.06 (43.75%) | 2.06 ±0.01 (56.25%) | | 8.50 ±0.03 | 5.52±0.04 |
| (Fe)PP-ZnO | 16.64 ±0.06 (19.04%) | 2.02 ±0.01 (26.67%) | 0.024 ±0.002 (54.29%) | 3.72 ±0.01 | 20.63±0.13 |
| (Cu)PP-ZnO | 16.98 ±0.05 (63.04%) | 2.06 ±0.01 (36.96%) | | 11.47 ±0.04 | 2.48±0.03 |

[a] The emission (monitored at 630 nm) was detected with 409 nm laser excitation. Numbers in parentheses indicate relative contributions.

in the presence of iron(III), the decay profile of PP-ZnO shows an additional time component of 0.024 ns (54.29%), which is not seen for either PP-ZnO or PP-ZnO in the presence of copper ions and can be rationalized as an electron migration pathway from PP to centrally located $Fe^{III}$.

### Photocatalytic degradation of methylene blue

To understand the modulation of the photocatalysis of PP-ZnO in the presence of dissolved metal ions under visible-light irradiation with our photodevice, as depicted in Figure 3, we performed in vitro photocatalysis measurements on a sample of the nanohybrid pre-doped with metal ions (12 h incubation time) in a quartz cuvette under visible light. The results are presented in Figure 7a. The inclusion of iron ions in the PP-ZnO nanohybrid significantly reduced the photocatalytic efficiency for the degradation of MB under visible-light irradiation compared to that in the case of the nanohybrid without metal ions or in the presence of copper ions. The relatively efficient photocatalysis by the nanohybrid containing copper ions may be correlated with the additional structural stability of the PP in this system.[14] Upon excitation with visible light, the sensitizer (PP) injects electrons into the conduction band (CB) of ZnO and the subsequent degradation of MB is initiated by CB electrons being transferred to it through reactive oxygen species (ROS). This sort of remote bleaching has been well-characterized in the literature. For example, Li et al. used porphyrin-sensitized $TiO_2$ photocatalysts to degrade acid chrome blue K, and the degradation mechanism was shown to follow an ROS pathway.[33] After one hour of visible-light irradiation, 55% of MB was degraded in the presence of PP-ZnO. However, the presence of copper(II) ions enhanced the photocatalytic activity and 80% MB degradation was observed. The copper(II) ions impart stability to the PP moiety attached to the ZnO NPs, which leads to enhancement of the photocatalytic activity. The photocatalytic activity of the PP-ZnO nanohybrid was significantly suppressed in the presence of iron(III) ions, and only 17% MB degradation was observed. In this case, the photoexcited electrons of PP were preferentially trapped in the $Fe^{III}$

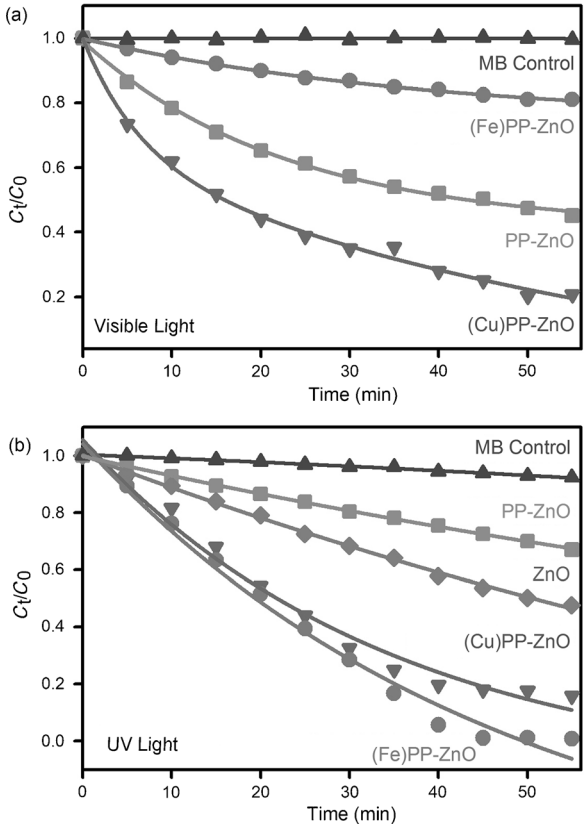


**Figure 7.** Photocatalytic degradation of MB in the presence of ZnO, PP-ZnO, (Fe)PP-ZnO, (Cu)PP-ZnO nanohybrids, and only MB under (a) visible-light and (b) UV irradiation.

ions rather than ZnO, which was evident from the transient absorption (Figure 5) and time-correlated single-photon counting (TCSPC) studies (Figure 6). This observation is consistent with the results obtained using the prototype flow device, as shown in Figure 3. Our transient absorption studies of the nanohybrid at 350 nm excitation revealed longer excitonic lifetimes in the presence of iron(III) ions compared to those obtained either without metal or in the presence of copper ions. As mentioned earlier, incorporation of iron in the central cavity of the porphyrin under UV light irradiation is expected to offer better photocatalysis than that in the case of visible-light irradiation. Another important factor is that any solar device should be exposed to the amount of UV radiation present in solar light (4–5%). Thus, in order to investigate the role of UV excitation, we studied the photocatalytic activity of the nanohybrid in the presence and absence of metal ions under UV irradiation, as shown in Figure 7b. Under UV irradiation, 55% MB degradation was observed in the presence of ZnO NPs, whereas only 25% MB degradation was observed in the presence of the PP-ZnO nanohybrid. Under UV irradiation, the ZnO valence band (VB) electrons are excited to the conduction band (CB) and can then reduce dioxygen to superoxide, eventually leading to the production of hydroxyl radicals (OH•). The hole in the valence band accepts electrons from water to generate hydroxyl radicals (OH•), which can also participate in the degradation process.[34] Thus, the efficiency of the nanohybrid essentially depends on the number of photogenerated carriers (electrons and holes) and their exciton lifetimes. In the case of (Fe)PP-ZnO, the photogenerated electron has been shown to be trapped in the centrally located iron moiety of the nanohybrid, and ROS generation is essentially governed by the hole in the valence band and the enhanced exciton lifetime (as evidenced from transient absorption, discussed above). On the other hand, for (Cu)PP-ZnO, ROS generation is expected to be governed by the photogenerated carriers (both electrons and holes), although it may not acquire any extra advantage from the exciton lifetime (as evidenced from transient absorption), revealing comparable photocatalysis to that in the (Fe)PP-ZnO nanohybrid. The significant retardation of photocatalysis in the case of PP-ZnO without metalation may be rationalized in terms of photoreduction of the attached PP by the photoexcited electron from ZnO. We have observed significant photobleaching of PP in PP-ZnO nanohybrids in the absence of metal ions under UV irradiation. The overall mechanistic pathway of the photocatalysis of the nanohybrid upon visible and UV irradiation is shown in Scheme 1.

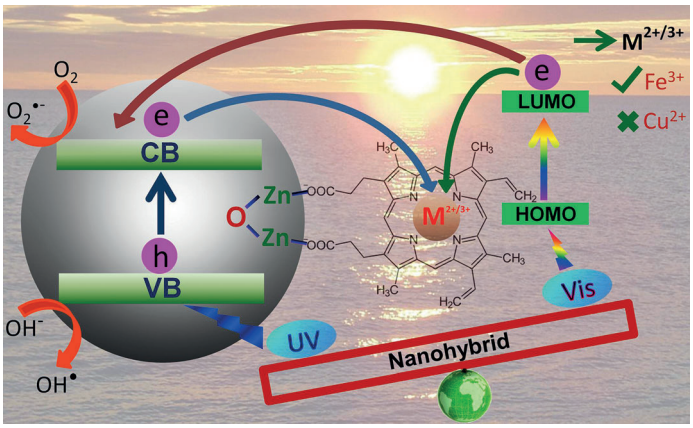


**Scheme 1.** Schematic representation of the ultrafast dynamic processes in a protoporphyrin-zinc oxide nanohybrid in the presence of different central metal ions under UV and visible-light excitation.

## Conclusion

We have synthesized and characterized a protoporphyrin IX-ZnO nanohybrid (PP-ZnO) for potential applications in a prototype photodevice for decontamination of test water with a model hazardous organic waste product from the textile industry. We have investigated the role of dissolved iron(III) and copper(II) ions in the test water based on their natural abundances (WHO prescribed). A number of microscopic and spectroscopic studies involving HRTEM, XRD, UV/Vis absorption, fluorescence, and FTIR have confirmed the structural integrity of the nanohybrid and the mode of attachment of the "green" PP to the ZnO host. Steady-state IR spectroscopy has provided conclusive experimental evidence for covalent attachment of PP to the host ZnO nanoparticles. On the other hand, our femtosecond-resolved transient absorption followed by picosecond-resolved fluorescence studies have clearly demonstrated that the residence of photoexcited electrons from the PP sensitizer in the centrally located iron moiety hinders ground-state bleach recovery of the sensitizer, affecting the overall photocatalytic efficiency of the nanohybrid. A schematic description of the mechanistic pathway in the nanohybrid upon UV and visible-light irradiation has also been presented. We envisage that this detailed spectroscopic study will potentially find relevance in the large-scale use of non-toxic and less expensive porphyrin-based nanohybrids for the decontamination of waste water.

## Experimental Section

Protoporphyrin IX (PP), zinc oxide nanoparticles (50 nm average size; ZnO NPs), copper(II) sulfate pentahydrate, and ferric(III) chloride were purchased from Sigma–Aldrich (USA). All other chemicals employed in the study were of analytical grade and were used without further purification.

### Sensitization of PP, $Fe^{III}PP$, and $Cu^{II}PP$ on the surface of ZnO NPs

A 0.5 mM PP ($C_{34}H_{36}N_4O_5$) solution was prepared in a mixture of dimethyl sulfoxide (DMSO) and deionized (DI) water (1:1, v/v) under constant stirring for 1 h. The ZnO NPs were sensitized with PP dye at room temperature in the dark by adding them to a 0.5 mM PP solution with continuous stirring for 12 h. After the sensitization process, the solution was centrifuged for a few minutes and the clear supernatant solution containing the unbound dye was removed. The sensitized material was then washed with DMSO/

water several times to remove any unbound dye. The nanohybrid was then dried by heating in a water bath and stored in the dark until further use. For the synthesis of $Fe^{III}$PP or $Cu^{II}$PP, we used 1:1 PP (0.5 mM) and metal ions (iron(III) chloride and copper(II) sulfate pentahydrate) in DMSO/water (1:1) and stirred the mixture for 12 h. After the metalation, the ZnO NPs were added to the $Fe^{III}$PP and $Cu^{II}$PP solutions and then stirred for a further 12 h. The prepared nanohybrids were washed several times with DMSO/water (1:1) to remove the unbound dye. The nanohybrids were dried by heating in a water bath and stored in the dark. We verified the dye loading by synthesizing the hybrids in a slightly different way. To this end, we first synthesized the PP-ZnO nanohybrids as described above and then added an equivalent of metal ions in DMSO/water (1:1) and stirred the resulting mixture for 12 h. The porphyrin loading was found to be the same as before. After washing, the nanohybrids were dried by heating in a water bath. We then performed the methylene blue degradation by using these nanohybrids and found that the results were similar to those shown in Figure 7.

### Characterization methods

Transmission electron microscopy (TEM) grids were prepared by applying a diluted drop of ZnO sample solution onto carbon-coated copper grids. The particle sizes were determined from micrographs recorded at a magnification of 100 000× using an FEI microscope (Tecnai S-Twin, operating at 200 kV). Energy-dispersive X-ray analysis spectra were acquired with a scanning electron microscope (SEM, JEOL JSM-6301 F, operating at 20 kV) for elemental analysis. For the optical experiments, the steady-state absorption and emission were determined with a Shimadzu UV-2450 spectrophotometer and a Jobin Yvon Fluoromax-3 fluorimeter, respectively. Picosecond-resolved spectroscopic studies were carried out using a commercial time-correlated single-photon counting (TCSPC) set-up from Edinburgh Instruments (instrument response function (IRF) = 80 ps, excitation at 409 nm). The observed fluorescence transients were fitted by using a nonlinear least-squares fitting procedure to a function, Equation (3):

$$(X(t) = \int_0^t E(t')R(t-t')dt') \tag{3}$$

comprising the convolution of the IRF ($E(t)$) with a sum of exponentials, Equation (4):

$$(R(t) = A + \sum_{i=1}^{N} B_i e^{-t/\tau_i}) \tag{4}$$

with pre-exponential factors ($B_i$), characteristic lifetimes ($\tau_i$), and a background (A). The relative concentration in a multi-exponential decay is finally expressed as Equation (5):

$$c_n = \frac{B_n}{\sum_{i=1}^{N} B_i} \times 100. \tag{5}$$

and the average lifetime (amplitude-weighted) of a multi-exponential decay is expressed as Equation (6):

$$\tau_{av} = \sum_{i=1}^{N} c_i \tau_i \tag{6}$$

FTIR spectra were recorded on a JASCO FTIR-6300 spectrometer, using a $CaF_2$ window.

### Femtosecond-resolved transient absorption study

In this study, a Helios UV/NIR femtosecond transient absorption spectroscopy system[35] was employed to measure transients of the samples. Helios is equipped with CMOS VIS and InGaAs NIR spectrometers covering the range 350–800 nm with 1.5 nm resolution at 9500 spectra $s^{-1}$ and the range 800–1600 nm with 3.5 nm resolution at 7900 spectra $s^{-1}$, respectively. The probe beam is provided by a Spectra-Physics Spitfire Pro 35 F-XP regenerative femtosecond amplifier, which produces 35 fs pulses at 800 nm with an energy of 4 mJ per pulse. A small portion (≈60 μJ) of the Spitfire output is routed via a delay line, adjustable pinholes, focusing lens, and a variable neutral density filter to a crystal for white light continuum (WLC) generation, and further to the sample via a focusing mirror. Two crystals are available to cover the Vis and NIR ranges. A computer-controlled delay line is used to vary the delay between the pump and probe pulses that allow transient absorption measurements within a 3.3 ns time window. A portion (1 mJ) of the Spitfire output is used to pump the TOPAS-C two-stage parametric amplifier equipped with frequency mixing stages and a non-colinear difference frequency generator that allows tuning from 240 to 2600 nm. The TOPAS-C output beam is routed via adjustable pinholes, a variable neutral density filter, a depolarizer, a chopper wheel, and a focusing lens to excite the sample. Pump and probe beams overlap spatially and temporally in the sample. The probe beam is collected by the spectrometer via collimating and focusing lenses and wave-pass filters to attenuate the white light around the Spitfire fundamental at 800 nm. All transient absorption experiments were conducted at room temperature. The observed transients were fitted using a nonlinear least-squares fitting procedure (SCIENTIST software) to a function composed of the convolution of the instrument response function with a sum of exponentials. The purpose of this fitting was to obtain the decays in an analytical form suitable for further data analysis.

### Photocatalysis by UV and visible light

In the photocatalysis study, PP-ZnO and (Fe)PP-ZnO and (Cu)PP-ZnO nanohybrids were dispersed in DI water and an aqueous solution of MB in DI water was used as the test contaminant. An 8 W UV source was used as the radiation source in this study. A high-pass optical filter (395 nm) was used for visible-light irradiation. The mixture of the photocatalyst and contaminant was irradiated for 1 h and the absorbance data were collected continuously by an Ocean Optics high-resolution spectrometer through a computer interface. The percentage of degradation (%DE) of MB was determined using Equation (7):

$$\%\,\mathrm{DE} = \frac{I_o - I}{I_o} \times 100 \tag{7}$$

in which $I_0$ is the initial absorption intensity of MB at $\lambda_{max} = 664$ nm, and $I$ is the absorption intensity after 1 h of continuous photoirradiation. In order to investigate the effect of metal ions present as impurities in water, a flow device was constructed to perform the photocatalysis. An in-house-constructed flow device consisting of two glass plates separated by a spacer was used to study the photocatalytic degradation of MB. One of the glass plates of the symmetric device contained the ZnO NPs sensitized with the PP dye.

As-prepared solutions of MB in DI water containing 0.07 mM $Fe^{3+}$ or 0.07 mM $Cu^{2+}$ were then injected through the flow device, which was placed under a visible-light source. The light was allowed to fall directly on the glass plate fabricated with PPIX-ZnO nanohybrids. The percentage of degradation (%DE) of MB was determined using Equation (7).

## Acknowledgements

The authors would like to acknowledge partial financial support from Umm Al-Qura University. The work is partially supported by King Abdullah University of Science and Technology. P.K. thanks the Council of Scientific and Industrial Research (CSIR, India) for fellowships. S.K.P. thanks the Department of Science and Technology (DST, India) for financial grants.

**Keywords:** femtochemistry · femtosecond transient absorption spectroscopy · nanohybrids · porphyrinoids · protoporphyrin IX

[1] a) B. O'Regan, M. Grätzel, *Nature* **1991**, *353*, 737 – 740; b) A. Fujishima, K. Honda, *Nature* **1972**, *238*, 37 – 38.
[2] a) H. Zhou, T. Fan, D. Zhang, *ChemSusChem* **2011**, *4*, 1344 – 1387; b) Y. Sun, Q. Wu, G. Shi, *Energy Environ. Sci.* **2011**, *4*, 1113 – 1132.
[3] L. M. Peter, *J. Phys. Chem. Lett.* **2011**, *2*, 1861 – 1867.
[4] a) J. N. Demas, D. Diemente, E. W. Harris, *J. Am. Chem. Soc.* **1973**, *95*, 6864 – 6865; b) S. L. Buell, J. N. Demas, *J. Phys. Chem.* **1983**, *87*, 4675 – 4681.
[5] J. W. Dobrucki, *J. Photochem. Photobiol. B* **2001**, *65*, 136 – 144.
[6] a) N. Robertson, *Angew. Chem.* **2006**, *118*, 2398 – 2405; *Angew. Chem. Int. Ed.* **2006**, *45*, 2338 – 2345; b) H. Hayashi, I. V. Lightcap, M. Tsujimoto, M. Takano, T. Umeyama, P. V. Kamat, H. Imahori, *J. Am. Chem. Soc.* **2011**, *133*, 7684 – 7687; c) A. Yella, H.-W. Lee, H. N. Tsao, C. Yi, A. K. Chandiran, M. K. Nazeeruddin, E. W.-G. Diau, C.-Y. Yeh, S. M. Zakeeruddin, M. Grätzel, *Science* **2011**, *334*, 629 – 634; d) L.-L. Li, E. W.-G. Diau, *Chem. Soc. Rev.* **2013**, *42*, 291 – 304; e) M.-y. Duan, J. Li, G. Mele, C. Wang, X.-f. Lü, G. Vasapollo, F.-x. Zhang, *J. Phys. Chem. C* **2010**, *114*, 7857 – 7862.
[7] Y. Chen, Z.-H. Huang, M. Yue, F. Kang, *Nanoscale* **2014**, *6*, 978 – 985.
[8] a) S. M. Reda, *Sol. Energy* **2007**, *81*, 755 – 760; b) J. A. Anta, E. Guillén, R. Tena-Zaera, *J. Phys. Chem. C* **2012**, *116*, 11413 – 11425; c) G. Granados-Oliveros, E. A. Páez-Mozo, F. M. Ortega, C. Ferronato, J.-M. Chovelon, *Appl. Catal. B* **2009**, *89*, 448 – 454.
[9] S. Sarkar, A. Makhal, T. Bora, K. Lakhsman, A. Singha, J. Dutta, S. K. Pal, *ACS Appl. Mater. Interfaces* **2012**, *4*, 7027 – 7035.
[10] J. Zhou, N. S. Xu, Z. L. Wang, *Adv. Mater.* **2006**, *18*, 2432 – 2435.
[11] a) W.-j. Sun, J. Li, G.-p. Yao, M. Jiang, F.-x. Zhang, *Catal. Commun.* **2011**, *16*, 90 – 93; b) T. Shiragami, J. Matsumoto, H. Inoue, M. Yasuda, *J. Photochem. Photobiol. C* **2005**, *6*, 227 – 248; c) W.-j. Sun, J. Li, G.-p. Yao, F.-x. Zhang, J.-L. Wang, *Appl. Surf. Sci.* **2011**, *258*, 940 – 945.
[12] H.-P. Lu, C.-Y. Tsai, W.-N. Yen, C.-P. Hsieh, C.-W. Lee, C.-Y. Yeh, E. W.-G. Diau, *J. Phys. Chem. C* **2009**, *113*, 20990 – 20997.
[13] E. M. Barea, V. Gónzalez-Pedro, T. Ripollés-Sanchis, H.-P. Wu, L.-L. Li, C.-Y. Yeh, E. W.-G. Diau, J. Bisquert, *J. Phys. Chem. C* **2011**, *115*, 10898 – 10902.
[14] S. Afzal, W. A. Daoud, S. J. Langford, *ACS Appl. Mater. Interfaces* **2013**, *5*, 4753 – 4759.
[15] M. K. Panda, K. Ladomenou, A. G. Coutsolelos, *Coord. Chem. Rev.* **2012**, *256*, 2601 – 2627.
[16] S. Sardar, S. Sarkar, M. T. Z. Myint, S. Al-Harthi, J. Dutta, S. K. Pal, *Phys. Chem. Chem. Phys.* **2013**, *15*, 18562 – 18570.
[17] N. Nasuha, B. H. Hameed, A. T. M. Din, *J. Hazard. Mater.* **2010**, *175*, 126 – 132.
[18] S. Fujihara, H. Naito, T. Kimura, *Thin Solid Films* **2001**, *389*, 227 – 232.
[19] A. McLaren, T. Valdes-Solis, G. Li, S. C. Tsang, *J. Am. Chem. Soc.* **2009**, *131*, 12540 – 12541.
[20] G. B. Deacon, R. J. Phillips, *Coord. Chem. Rev.* **1980**, *33*, 227 – 250.
[21] a) W. Tu, J. Lei, P. Wang, H. Ju, *Chem. Eur. J.* **2011**, *17*, 9440 – 9447; b) P. Jiang, J. J. Zhou, H. F. Fang, C. Y. Wang, Z. L. Wang, S. S. Xie, *Adv. Funct. Mater.* **2007**, *17*, 1303 – 1310.
[22] a) E. Collini, C. Ferrante, R. Bozio, *J. Phys. Chem. B* **2005**, *109*, 2 – 5; b) S. Verma, A. Ghosh, A. Das, H. N. Ghosh, *J. Phys. Chem. B* **2010**, *114*, 8327 – 8334.
[23] G. Mele, R. Sole, G. Vasapollo, E. García-López, L. Palmisano, L. Jun, R. Słota, G. Dyrda, *Res. Chem. Intermed.* **2007**, *33*, 433 – 448.
[24] S. G. Kruglik, P. A. Apanasevich, V. S. Chirvony, V. V. Kvach, V. A. Orlovich, *J. Phys. Chem.* **1995**, *99*, 2978 – 2995.
[25] D. Kim, D. Holten, M. Gouterman, *J. Am. Chem. Soc.* **1984**, *106*, 2793 – 2798.
[26] S. Sarkar, A. Makhal, S. Baruah, M. A. Mahmood, J. Dutta, S. K. Pal, *J. Phys. Chem. C* **2012**, *116*, 9608 – 9615.
[27] a) C. Yogi, K. Kojima, N. Wada, H. Tokumoto, T. Takai, T. Mizoguchi, H. Tamiaki, *Thin Solid Films* **2008**, *516*, 5881 – 5884; b) A. Mills, J. Wang, *J. Photochem. Photobiol. A* **1999**, *127*, 123 – 134.
[28] E. B. Fleischer, E. I. Choi, P. Hambright, A. Stone, *Inorg. Chem.* **1964**, *3*, 1284 – 1287.
[29] P. Castillero, J. R. Sánchez-Valencia, M. Cano, J. M. Pedrosa, J. Roales, A. Barranco, A. n. R. González-Elipe, *ACS Appl. Mater. Interfaces* **2010**, *2*, 712 – 721.
[30] H. Huang, X. Gu, J. Zhou, K. Ji, H. Liu, Y. Feng, *Catal. Commun.* **2009**, *11*, 58 – 61.
[31] A. Kongkanand, K. Tvrdy, K. Takechi, M. Kuno, P. V. Kamat, *J. Am. Chem. Soc.* **2008**, *130*, 4007 – 4015.
[32] A. Kathiravan, P. S. Kumar, R. Renganathan, S. Anandan, *Colloids Surf. A* **2009**, *333*, 175 – 181.
[33] D. Li, W. Dong, S. Sun, Z. Shi, S. Feng, *J. Phys. Chem. C* **2008**, *112*, 14878 – 14882.
[34] M. R. Hoffmann, S. T. Martin, W. Choi, D. W. Bahnemann, *Chem. Rev.* **1995**, *95*, 69 – 96.
[35] J. Sun, W. Yu, A. Usman, T. T. Isimjan, S. DGobbo, E. Alarousu, K. Takanabe, O. F. Mohammed, *J. Phys. Chem. Lett.* **2014**, *5*, 659 – 665.

Received: March 17, 2014
Published online on July 10, 2014